Materializing a binary hyperlens design

Alexander V. Kildishev,[a] Uday K. Chettiar, Zubin Jacob, Vladimir M. Shalaev, and Evgenii E. Narimanov
Birck Nanotechnology Center, School of Electrical and Computer Engineering, Purdue University, West Lafayette, Indiana 47907, USA

(Received 23 December 2008; accepted 17 January 2009; published online 17 February 2009)

We present a design of cylindrical hyperlens made of a layered binary material. The design approach uses an improved effective medium theory to take account of radius-dependent effects due to curvature of material interfaces resulting in nonperiodically distributed thicknesses of the lens layers. The performance of this lens is compared versus the designs with periodically thick layers, which we showed in earlier papers. Detailed quantitative results analyzed for the lenses with the same number and starting order of layers prove better functioning of the lens designed with this approach. © *2009 American Institute of Physics*. [DOI: 10.1063/1.3081403]

The recent advancement theory of hyperlens and enhanced nanofabrication techniques have provided us with a fresh perspective on magnifying subwavelength imaging devices made of anisotropic materials with hyperbolic dispersion.[1,2] In prefabrication design and experiments the required anisotropy was achieved through the fabrication of a cylindrical lamellar structure made of two distinct elementary materials (i.e., a binary metal-dielectric composite). A periodic distribution of metal-dielectric layers of a fixed thickness has been used. The focus of our study is (i) how to quantify, at least in quasistatic limit, the genuinely curvilinear interfaces of the cylindrical hyperlens in a radius-dependent effective medium theory (EMT) and (ii) if this EMT could improve the performance of the cylindrical hyperlens. The initial analysis indicated that a nonperiodic distribution of thicknesses of the lens layers is required for the improved design. Detailed simulations prove superior functioning of the lens designed with the improved approach versus the designs with the uniformly thick layers if the same number and starting order of layers is taken. The numerical analysis is built on the solution of the wave equation in piecewise homogeneous cylindrical coordinates, which has been widely detailed in literature.[3] Our study is using the scalar wave equation; the electric field is assumed to be two-dimensional and the magnetic field is the purely scalar quantity. For TM polarization the magnetic field (parallel to $\vec{H}=\hat{\mathbf{z}}h$) can be expanded in azimuthal Fourier modes, $h(\rho,\phi)=\Sigma h_m(\rho)\exp \imath m\phi$ and the wave equation for the mth mode reduces to

$$\varepsilon_\rho \rho^{-1}(\rho\varepsilon_\phi^{-1}h_m')' + [k^2\varepsilon_\rho\mu_z - (m/\rho)^2]h_m = 0. \quad (1)$$

Here the physical Cartesian coordinates (x,y,z) are defined through the cylindrical coordinates (ρ,ϕ,z) as $x=\rho\cos(\phi)$, $y=\rho\sin(\phi)$, and $z=z$; the prime corresponds to the radial derivative $\partial/\partial\rho$, ε_ρ and ε_ϕ are the only nonzero diagonal components of the anisotropic permittivity tensor, and k is the wavenumber of free-space. While the ideal and simplified hyperlens paradigms[2,4] are based on smooth scaling transformations[5] of Eq. (1), the proposed design of a manufacturable discrete-layered cylindrical hyperlens does not yet imply quantum size effects and other complications at the metal-dielectric interfaces, and thus each layer is taken to have isotropic dielectric function ($\varepsilon_\rho=\varepsilon_\phi$). The transformation of field data within each cylindrical layer to another place is accomplished by representing the field as a summation of spatial harmonics. The harmonic coefficients are determined by matching the fields at the interfaces with the expansion solution of the wave equation. Once these coefficients are found, the field is computed everywhere by using the sums of spatial harmonics. Making use of the cylindrical mode superposition, the source field and scattered fields are decomposed into backward (inbound) and forward (outbound) modes. The transfer matrices are deduced directly from Maxwell equations and are cast in a spatial spectral form and then in matrix relations. Test problems are simulated using our *ad hoc* online tool,[6] where the hyperlens may consist of any number of layers bounded by infinite concentric cylindrical surfaces. The material properties of the media layers are utilizing the material optical database[7] where the materials are allowed to be dispersive, embracing polaritonic (plasmonic or phononic) media. Consider a classical hyperlens [a circular cylindrical multilayered structure comprising $l_{\max}$ cylindrical interfaces of lamellar media (Fig. 1)]. The axes of concentric cylindrical surfaces are assumed to coincide with the z-axis of a common cylindrical coordinate system (ρ,ϕ,z). Each interface boundary with a radius ρ_l separates two homogeneous media with the constant permeability $\mu=1$ and a pair of dielectric functions, ε_l and ε_{l+1}. In TM formulation for a fixed free-space wavelength λ, the scalar magnetic field for a given lth interface is described by four components: the transmitted (h_t^{2l}) and reflected (h_r^{2l}) field at

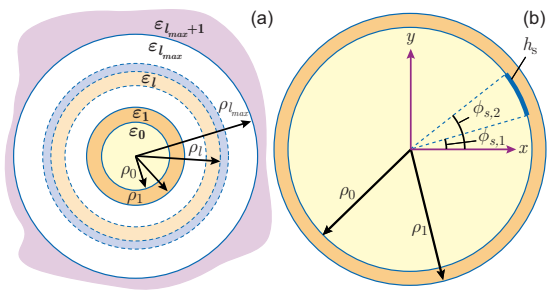

FIG. 1. (Color online) (a) Geometry of the concentric circular domains. (b) Example of the test source inside the zoomed internal region of the lens.

[a]Electronic mail: kildishev@purdue.edu.

the inner side of the boundary, h_t^{2l} and h_r^{2l} field at the inner side of the boundary

$$h_t^{2l} = \sum t_m^l e^{um\phi}, \quad h_r^{2l} = \sum r_m^l e^{um\phi}, \tag{2}$$

and the transmitted (h_t^{2l+1}) and reflected (h_r^{2l+1}) fields at the outer side of the interface boundary

$$h_t^{2l+1} = \sum t_m^{l+1} \bar{f}_m^l e^{um\phi}, \quad h_r^{2l+1} = \sum r_m^{l+1} \bar{b}_m^l e^{um\phi}, \tag{3}$$

where factors $\bar{f}_m^l = f_m^{2l+1}/f_m^{2l+2}$, $\bar{b}_m^l = b_m^{2l+1}/b_m^{2l+2}$ can be defined using the forward $[f_m^{(.)}]$ and backward $[b_m^{(.)}]$ radial functions are the Hankel and Bessel cylindrical functions of the first kind. Thus, the even and odd terms are given by $f_m^{2l} = H_m^{(1)} \times (\rho_l)$, $b_m^{2l} = J_m(\rho_l)$ and $f_m^{2l+1} = H_m^{(1)}(q_l)$, $b_m^{2l+1}(\rho) = J_m(q_l)$ (their derivatives are given as $f_m'^{2l} = \partial H_m^{(1)}(\rho_l)/\partial \rho_l$, $b_m'^{2l} = \partial J_m(\rho_l)/\partial \rho_l$ and $f_m'^{2l+1} = \partial H_m^{(1)}(q_l)/\partial q_l$, $b_m'^{2l+1} = \partial J_m(q_l)/\partial q_l$ for $p_l = n_l \bar{\rho}_l$ and $q_l = n_{l+1}\bar{\rho}_l$). Here, $n_l = \sqrt{\varepsilon_l}$ is the refractive index of the medium adjacent to the inner side of the lth interface and $\bar{\rho}_l = 2\pi\rho_l/\lambda$ is a wavelength-normalized radius. The sums in Eqs. (1) and (2) and in equations below are generally defined as summations over $m = (-\infty, \infty)$.

For testing, the incident field can be, for example, generated by an expansion of the step-function, forcing the incident field to be unity at an arc segment with a constant radius ρ_s and angular dimensions $\phi = [\phi_{s,1}, \phi_{s,2}]$ [Fig. 1(b)]. If we apply the complete version of the same addition theorem in $h_i = H_0^{(1)}(k\rho_i) m_s$, then the incident field is given either by $h_t^0 = \Sigma t_m^0 e^{um\phi}$ (for sources distributed inside the lens, $\rho > \rho_s$) or by $h_r^{2l_{\max}+1} = \Sigma r_m^{l_{\max}+1} e^{um\phi}$ (for external sources, $\rho_s > \rho$). Then, for $\rho_s < \rho_0$, $t_m^0 = \psi_m$, as well as $r_m^{l_{\max}+1} = \psi_m$ for $\rho_s > \rho_{l_{\max}}$, where for $m > 0$, $\psi_m = (e^{-um\phi_{s,2}} - e^{-um\phi_{s,1}})[um(\phi_{s,2} - \phi_{s,1})]^{-1}$, while otherwise, $\psi_0 = 1$. In practice of designing engineered optical spaces, a smooth ideal distribution is approximated by a few elemental materials. Thus normally, subwavelength thin layers of dispersive and nondispersive elemental materials should be arranged to provide desired effective properties. The effective material properties of a planar binary-phase cylindrical structure can be obtained from the following quasistatic approximations:

$$\varepsilon_{\rho,l}^{-1} \ln\frac{\rho_{l+2}}{\rho_l} = \varepsilon_l^{-1} \ln\frac{\rho_{l+1}}{\rho_l} + \varepsilon_{l+1}^{-1} \ln\frac{\rho_{l+2}}{\rho_{l+1}}, \tag{4}$$

$$\varepsilon_{\phi,l} \ln\frac{\rho_{l+2}}{\rho_l} = \varepsilon_l \ln\frac{\rho_{l+1}}{\rho_l} + \varepsilon_{l+1} \ln\frac{\rho_{l+2}}{\rho_{l+1}}. \tag{5}$$

Since $\ln(1+x) \approx x + O(x^2)$, then for very thin layers the above relapses into familiar expressions for the effective permittivity of a planar lamellar structure,

$$\varepsilon_{\rho,l}^{-1} = \varepsilon_l^{-1} \frac{\rho_{l+1} - \rho_l}{\rho_{l+2} - \rho_l} + \varepsilon_{l+1}^{-1} \frac{\rho_{l+2} - \rho_{l+1}}{\rho_{l+2} - \rho_l}, \tag{6}$$

$$\varepsilon_{\phi,l} = \varepsilon_l \frac{\rho_{l+1} - \rho_l}{\rho_{l+2} - \rho_l} + \varepsilon_{l+1} \frac{\rho_{l+2} - \rho_{l+1}}{\rho_{l+2} - \rho_l}, \tag{7}$$

which could be also used as an effective medium approximation. It is essential to understand which of the two formulations, Eqs. (3) and (4) or Eqs. (5) and (6), provides a better performance of a binary circular hyperlens.

Field-matching boundary conditions at lth interface are given by $h_t^{2l} + h_r^{2l} = h_t^{2l+1} + h_r^{2l+1}$, $n_l^{-1}\partial(h_t^{2l} + h_r^{2l})/\partial p_l = n_{l+1}^{-1}\partial(h_t^{2l+1} + h_r^{2l+1})/\partial q_l$. The above system of equations can be rewritten using a matrix notation $\mathbf{v}_{l,m} = \mathbf{w}_{l,m}\mathbf{v}_{l+1,m}$, with the components of vector $\mathbf{v}_m^l$ being $(\mathbf{v}_m^l)_0 = t_m^l$ and $(\mathbf{v}_m^l)_1 = r_m^l$, while the elements of matrix $\mathbf{w}_{l,m}$ are given by $w_{l,m}^{1,1} = \tau_m \bar{f}_m^l (l_{f,m}^{2l+1} - l_{b,m}^{2l})$, $w_{l,m}^{2,1} = \tau_m \bar{f}_m^l (l_{f,m}^{2l} - l_{f,m}^{2l+1})$, $w_{l,m}^{1,2} = \tau_m \bar{b}_m^l (l_{b,m}^{2l+1} - l_{b,m}^{2l})$, and $w_{l,m}^{2,2} = N_l \bar{b}_m^l (l_{f,m}^{2l} - l_{b,m}^{2l+1})$, where $l_{f,m}^{2l+1} = n_{l+1}^{-1} ln' f_m^{2l+1}$, $l_{b,m}^{2l} = n_l^{-1} ln' b_m^{2l}$, $l_{f,m}^{2l} = n_l^{-1} ln' f_m^{2l}$, and $\tau_{l,m} = \frac{1}{2} \iota\pi n_l^2 \bar{\rho}_l f_m^{2l} b_m^{2l}$. Finally, cascading elementary layers (Fig. 1) gives $\mathbf{v}_m^0 = \overline{\mathbf{w}}_m \mathbf{v}_m^{l_{\max}+1}$ and $\overline{\mathbf{w}}_m = \Pi_{l=1}^{l_{\max}} \mathbf{w}_{l,m}$. If the ratios $\bar{r}_m^l = r_m^l / t_m^l$ and $\bar{t}_m^l = t_m^{l_{\max}+1} / t_m^l$ are initialized with $\bar{t}_m^{l_{\max}+1} = 1$ and $\bar{t}_m^{l_{\max}+1} = 1$, then in a multilayer structure the normalized spatial spectral reflectance and transmittance are obtained through the following recurrences: $\bar{r}_m^l = (w_{l,m}^{2,1} + w_{l,m}^{2,2}\bar{r}_m^{l+1})/\bar{\tau}_m^l$ and $\bar{t}_m^l = \bar{t}_m^{l+1}/\bar{\tau}_m^l$, where $\bar{\tau}_m^l = w_{l,m}^{1,1} + w_{l,m}^{1,2}\bar{r}_m^{l+1}$.

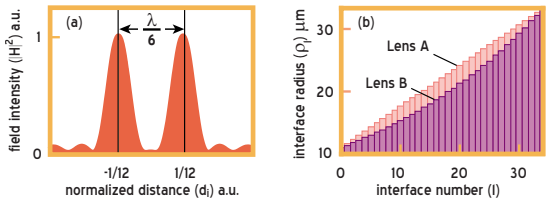

FIG. 2. (Color online) (a) Input magnetic field intensity at ρ_0 used for all tests. (b) Comparison of the nonuniform distribution of $\rho_{l_{\max}}$ obtained from Eq. (9) vs the uniform distribution; $l_{\max} = 34$ has been taken for this example.

The performance of the hyperlens is tested for two designs, proposed for two elemental materials SiC and ZnSe to be operational at a wavelength of $\lambda = 11.061$ μm, with $\varepsilon_{\text{SiC}} = -4.5 + \iota 0.271$, and $\varepsilon_{\text{ZnSe}} = 5.5$. Note that at this wavelength both dielectric functions satisfy the condition $\text{Re}(\varepsilon_{\text{SiC}} + \varepsilon_{\text{ZnSe}}) = 1$, providing good balance of elemental materials in the structure. The first design (lens A) is arranged with uniformly spaced interfaces, which in accord with Eqs. (5) and (6) would give constant values of $\text{Re}(\varepsilon_{\phi,l}) = 1$ and $\text{Re}(\varepsilon_{\rho,l}) \sim 10$. Though as shown in Fig. 2, lens A gives staggered values of $\varepsilon_{\rho,l}$ and $\varepsilon_{\phi,l}$ if calculated for the same uniform layers with Eqs. (3) and (4). In contrast to lens A, lens B is also obtained by fixing $\text{Re}(\varepsilon_{\phi,l}) = 1$ for each two sequential layers (ZnSe–SiC or SiC–ZnSe) but without fixing $\text{Re}(\varepsilon_{\rho,l})$. This design rule defines the following three term recurrence for interface radii:

$$\rho_{l+1} = \rho_l (\rho_{l-1}/\rho_l)^{(\text{Re}(\varepsilon_l)-1)/(\text{Re}(\varepsilon_{l+1})-1)}. \tag{8}$$

Thus for a given number of layers $l_{\max}$ in lens B, the entire design is achieved through adjusting the sequence of radii in order to fit the outer radius $\rho_{l_{\max}}$.

While compared, both lens designs share a common set of dimensions, $\rho_0 = \lambda$, and $\rho_{l_{\max}} = 3\lambda$, and the same number of elementary layers. It has been observed that a lens with nonuniform thicknesses of layers, lens B always gives a better resolution in comparison with lens A with the same number of layers, and the best performance for lens B is achieved with the odd number of layers with the inner layer made of metal (SiC–ZnSe sequence). For example, Fig. 3 compares imaging with lens A versus lens B; the normalized distance in Fig. 3 is defined as $d_e = \rho_{l_{\max}}\phi/\lambda$. For both lenses, the test image is obtained with the best-performing order of elementary layers (SiC–ZnSe for $l_{\max} = 31$ and ZnSe–SiC for $l_{\max} = 32$). Figures 3(b) and 3(d) show that lens B is already working quite well even for such small numbers of layers,

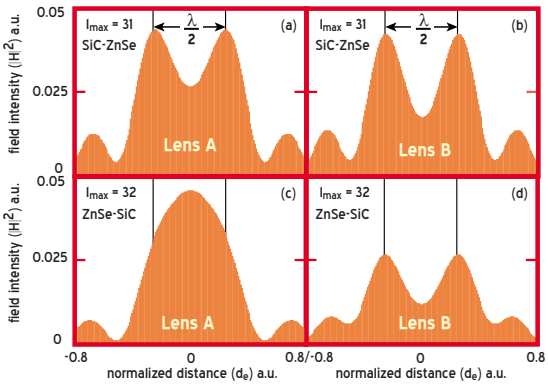

FIG. 3. (Color online) Output image from lens A vs the image from lens B obtained at the output boundary. (a) Lens A with 31 layers and the initial order of layers is SiC–ZnSe. (c) Lens A with 32 layers; the initial order of layers is ZnSe–SiC. [(b) and (d)] Same as (a) and (c) but for lens B.

while lens A is barely resolving the image [Fig. 3(c)] or does not resolve it at all [Fig. 3(d)].

In the past few years, an improved EMT has been applied to obtain nonlocal corrections to the quasistatic EMT of anisotropic materials made of lamellar structures with subwavelength-thick layers.[8] Thus, a near term work could include the incorporation of nonlocal adjustments for cylindrical system in a way much similar to the techniques introduced for planar structures.

This work was supported in part by ARO under Grant No. W911NF-04-1-0350 and by ARO-MURI award under Grant No. 50342-PH-MUR.

[1]Z. Jacob, L. V. Alekseyev, and E. Narimanov, J. Opt. Soc. Am. A Opt. Image Sci. Vis **24**, A52 (2007); Y. Xiong, Z. Liu, C. Sun, and X. Zhang, Nano Lett. **7**, 3360 (2007); X. Zhang and Z. W. Liu, Nature Mater. **7**, 435 (2008).
[2]A. V. Kildishev and E. E. Narimanov, Opt. Lett. **32**, 3432 (2007).
[3]E. G. Post, *Formal Structure of Electromagnetics; General Covariance and Electromagnetics* (Interscience, New York, 1962), p. 204.
[4]Z. Jacob, L. V. Alekseyev, and E. Narimanov, Opt. Express **14**, 8247 (2006).
[5]L. S. Dolin, Izv. Vyssh. Uchebn. Zaved., Radiofiz. **4**, 964 (1961); A. J. Ward and J. B. Pendry, Phys. Rev. B **58**, 7252 (1998); M. Lax and D. F. Nelson, *ibid.* **13**, 1777 (1976); D. Schurig, J. B. Pendry, and D. R. Smith, Opt. Express **15**, 14772 (2007); A. V. Kildishev and V. M. Shalaev, Opt. Lett. **33**, 43 (2008).
[6]M. Swanson, A. V. Kildishev, and X. Ni, "Hyperlens layer designer" (unpublished), doi: 10254/nanohub-r4703.1; M. Swanson, X. Ni, Z. Jacob, and A. V. Kildishev, "Hyperlens design solver" (unpublished), doi: 10254/nanohub-r4770.2, http://www.nanohub.org/tools/hypiesolver.
[7]X. Ni, Z. Liu, and A. V. Kildishev, "PhotonicsDB: Optical constants" (unpublished), doi: 10254/nanohub-r3692.1.
[8]I. Avrutsky, J. Opt. Soc. Am. A Opt. Image Sci. Vis **20**, 548 (2003); J. Elser, V. A. Podolskiy, I. Salakhutdinov, and I. Avrutsky, Appl. Phys. Lett. **90**, 191109 (2007).